ADVANCED OPTICAL MATERIALS
www.advopticalmat.de

Empirical Comparison of Random and Periodic Surface Light-Trapping Structures for Ultrathin Silicon Photovoltaics

*Matthew S. Branham, Wei-Chun Hsu, Selcuk Yerci, James Loomis, Svetlana V. Boriskina, Brittany R. Hoard, Sang Eon Han, Abasifreke Ebong, and Gang Chen**

Dramatic reductions in the production cost of wafer-based mono- and multicrystalline silicon solar cells have fueled the photovoltaic industry, with these two technologies accounting for a combined 90% of the 39.8 GW solar module market in 2013.[1] As additional cost reductions become progressively more challenging, the push to find transformative alternatives has intensified. One promising approach is to radically reduce the amount of silicon in a device — which constitute 30%–40% of module cost[2,3]— by moving from wafers to ultrathin crystalline silicon films with absorber layers thinner than 20 µm. One potential drawback of thin crystalline silicon is reduced photocurrent — and therefore efficiency — resulting from weak absorption of long-wavelength radiation, a consequence of silicon's indirect bandgap. Researchers have addressed this challenge by developing strategies to control the transport of radiative energy in a thin silicon absorber, "trapping" the light in the film and increasing the absorption probability so as to improve overall solar cell performance.

The concept of light trapping is not a new one. In 1974, Redfield introduced a solar cell design making use of angled features to increase the number of passes a photon makes through the absorber.[4] In the 1980s, random pyramid texturing was pioneered by etching silicon in a weak alkaline/isopropyl alcohol (IPA) solution, becoming the de facto standard for absorption enhancement in wafer-based crystalline silicon solar cells.[5] More recently, ultrathin silicon photovoltaic (PV) concepts have generated renewed interest in the design of light-trapping structures. It is typically assumed that conventional random pyramid surface textures are inappropriate for ultrathin films because the volume of silicon removed during etching would compromise overall absorption. Nanophotonic light-trapping designs seek to address this issue by exploiting photon transport in the wave optics regime to yield superior absorbers with minimal silicon removal. A great variety of nanophotonic surface light-trapping geometries have been proposed, such as nanoholes and nanocylinders,[6–8] nanocones and nanodomes,[9–12] inverted nanopyramids,[13–15] nanowires,[16–19] and more complex parametric designs.[20–22] See ref.[23] for an excellent review of light-trapping designs for thin silicon photovoltaic devices. Other light-trapping approaches include Bragg reflectors integrated with rear diffraction gratings[24,25] and nanoparticles for plasmonic scattering and enhanced absorption.[26–31] Owing to the difficulties of simulation and fabrication, generally absent from the literature is a demonstration of how nanophotonic structures fare in practice compared to random pyramid surface textures that are the standard in industry as well as to light-trapping designs with larger feature sizes.

In this article, we focus on inverted nanopyramids as archetypal light-trapping structures that have also been shown to be among the best-performing nanophotonic light-trapping designs[13,14,23] and combine the results of experiment and simulation to investigate two questions: (1) do wavelength-scale features offer superior broad spectrum absorption compared to larger structures and (2) how do conventional random pyramid surface textures compare with periodic nanophotonic light-trapping designs? In contrast with common assumptions, we show that inverted pyramids larger than 1 µm in pitch perform as well or better than submicrometer nanophotonic designs. Similarly, experimental results indicate that ultrathin silicon films textured with periodic inverted pyramid (PIP) arrays absorb as effectively as those with random upright pyramids (UPs). The crucial point, however, is that absorption in thin silicon films is very high for each type of pyramidally textured surface compared to the Yablonovitch limit, which is in part a function of the near ideal slope of pyramids formed by the etching of (100) silicon in alkaline solutions.

Commonly, the absorption efficiency of a light-trapping design is referenced to the Yablonovitch limit and to a planar, untextured reference as upper and lower bounds of performance, respectively. The Yablonovitch limit defines the upper bound for absorption (A) in a material when light propagation can be described in terms of geometric optics.[32,33] For a material slab with perfect antireflection and isotropic scattering at both the top and bottom surfaces, the limit is given as[32,34]

Dr. M. S. Branham, W.-C. Hsu, Dr. S. V. Boriskina, Prof. G. Chen
Department of Mechanical Engineering
Massachusetts Institute of Technology
77 Massachusetts Ave, Cambridge, MA 02139, USA
E-mail: gchen2@mit.edu
Prof. S. Yerci
Micro and Nanotechnology Programme
The Center for Solar Energy Research and Applications
Department of Electrical and Electronics Engineering
Middle East Technical University
Dumlupinar Blv, No. 1, 06800 Cankaya, Ankara, Turkey
Dr. J. Loomis
Department of Mechanical Engineering
The University of Auckland
Auckland, New Zealand
B. R. Hoard, Prof. S. E. Han
Department of Chemical and Biological Engineering
The University of New Mexico
1 University of New Mexico, Albuquerque, NM 87131, USA
Prof. A. Ebong
Electrical and Computer Engineering Department
The University of North Carolina at Charlotte
Charlotte, NC 28223, USA

DOI: 10.1002/adom.201500667

$$A = \frac{1 - e^{-4\alpha\ell}}{1 - \left(1 - \frac{1}{n^2}\right)e^{-4\alpha\ell}} \quad (1)$$

where the attenuation coefficient $\alpha = 4\pi\kappa\lambda^{-1}$, n and κ are the real and imaginary refractive indices, respectively, λ denotes wavelength, and ℓ is the material thickness. Although originally derived through statistical mechanics, the Yablonovitch limit can also be recovered from the thermodynamic upper bound for absorption in a solid film with the identical assumption of isotropic surface scattering in a bulk medium.[35] Critically, this limit does not hold in the case of subwavelength-scale film thicknesses or in the presence of subwavelength-scale geometric inclusions.[36,37] Researchers have sought to harness wave optics effects to design structures exceeding the Yablonovitch limit with the goal of producing efficient silicon photovoltaics while using much less silicon than is conventionally required.

We fabricated physical samples on 5, 10, and 20 µm silicon films with four different surface morphologies: (1) randomly sized and spaced UPs, 2D PIPs with periods of (2) 700 nm and (3) 2.2 µm, and (4) polished planar (**Figure 1**a–d). Each sample was coated on the top surface with silicon nitride deposited by plasma-enhanced chemical vapor deposition (PECVD), and the rear was coated with a silicon dioxide/aluminum reflector stack. Before proceeding, it should be emphasized that the experimental data presented in this article measures total absorption, which includes absorption in silicon as well as parasitic absorption in the aluminum reflector and nitride layer. We assume that to first order the impact of parasitic photon absorption is comparable between textured samples.

The spectral details of the samples' absorption characteristics reveal subtle, informative differences between the surface structures for substrates of 5, 10, and 20 µm thickness, respectively (Figure 1e–g). Virtually all of the periodic and random-pyramid-textured samples absorb extremely well for $500 < \lambda < 800$ nm, where they primarily serve to limit surface reflection, generally capturing 95%–99% of all photons in this range for all sample types. This portion of the solar spectrum also contains the highest density of photons, with about half (20.8 mA cm^{-2}) of the 43.7 mA cm^{-2} total current potential between $300 < \lambda \leq 1105$ nm falling in this range. Outside of $500 < \lambda < 800$ nm, the differences in spectral absorption that can be seen from one textured sample type to another for a given silicon thickness arise from differences in feature size of the surface textures and attendant geometric variation as well as experimental variation between samples. For example, earlier studies have shown that reflection from the top surface increases in the short wavelength range ($300 < \lambda < 500$ nm) as the width of the ridge, w, separating one pyramid from another increases (Figure S1, Supporting Information).[13] This effect can be understood by considering that the fixed pitch of the pyramids requires that, for larger ridge widths, the proportion of surface area that is normal to incident photons is greater.

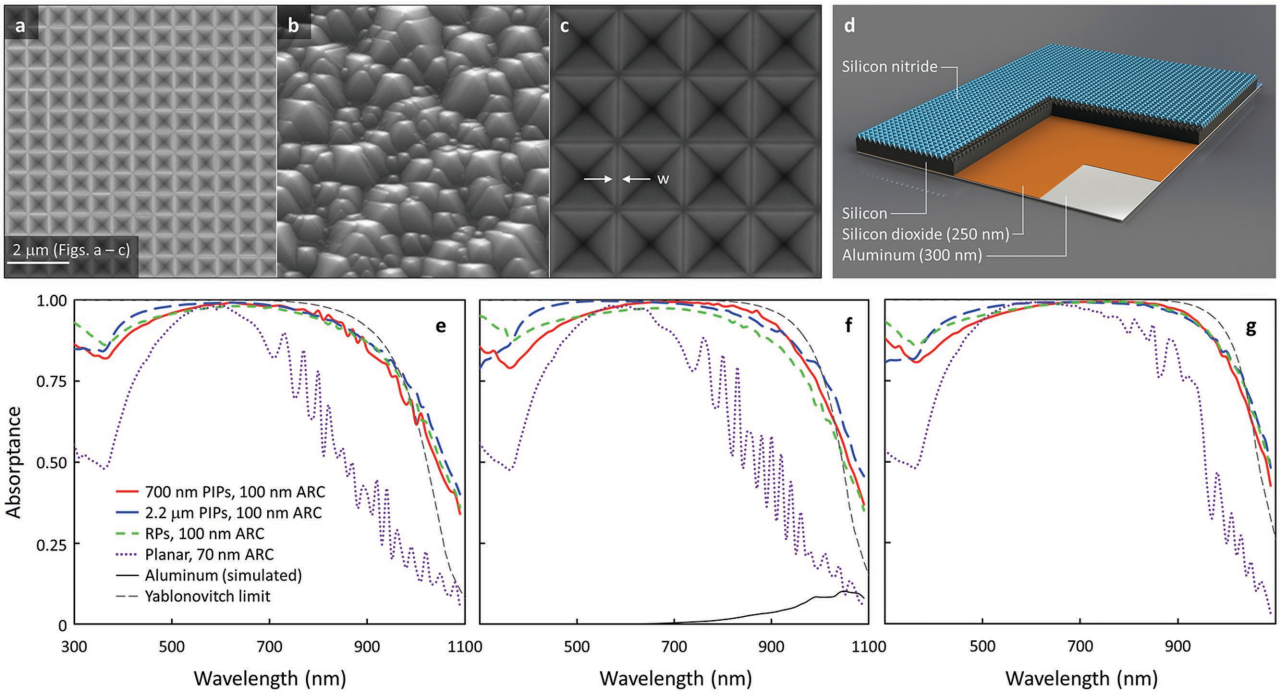

Figure 1. Scanning electron microscope (SEM) images of a) 700 nm pitch periodic inverted pyramids, b) randomly sized and spaced upright pyramids, and c) 2.2 µm pitch periodic inverted pyramids. The pyramid ridge width, w, is defined in (c). d) Schematic of the textured samples. Absorption spectra for silicon films e) 5 µm, f) 10 µm, and g) 20 µm thick with surfaces textured with periodic inverted pyramids on 700 nm and 2.2 µm pitches, random upright pyramids, and planar surfaces for comparison. Each sample has a 250 nm thick back oxide and a rear aluminum reflector. The thickness of the surface nitride anti-reflection coating (ARC)—optimized separately for textured (100 nm) and planar (70 nm) surfaces—is provided in the legend. Parasitic absorption (from simulation) in the rear aluminum reflector is plotted in (f) for a 10 µm silicon sample with the structure shown in (d). The Yablonovitch limit is plotted for a silicon slab of the same film thickness assuming zero front surface reflection and unity back surface reflection.

Adv. Optical Mater. **2016**,
DOI: 10.1002/adom.201500667

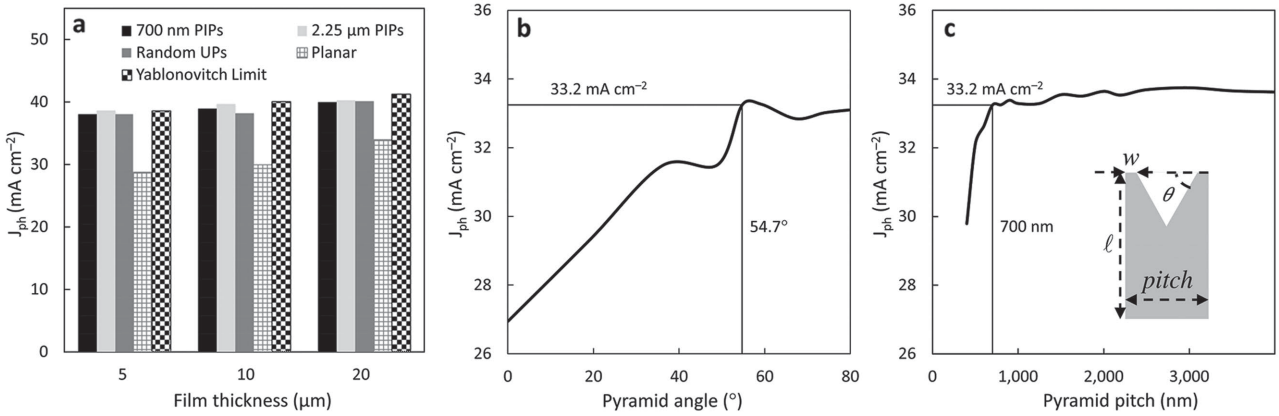

Figure 2. a) Average experimentally measured total integrated spectral absorptivity, expressed in terms of J_{ph}, for silicon films of 5, 10, and 20 μm thickness with random UP and PIP surface textures. The standard deviation for all experimental sample types is less than 0.4 mA cm^{-2}. 3D finite element analysis (FEA) simulation (COMSOL Multiphysics software) of total integrated absorption in silicon ($300 < \lambda < 1105$ nm) for an ultrathin silicon film as a function of the b) angle and c) pitch of the inverted pyramid surface texturing. The simulated film structure is the same as Figure 1d, with a textured silicon film sandwiched between a 100 nm PECVD silicon nitride layer on the top surface and 250 nm silicon dioxide layer below. The back reflector is 300 nm aluminum. Silicon film thickness is 10 μm; ridge width (w) is fixed at 50 nm.

Blue photons can better "see" these narrow regions of the surface by virtue of their short wavelength, and since the normal surface area presents a more abrupt index change, reflection increases. As a result of the constraints of the fabrication process, the ridge width for the 700 nm PIPs is ≈50–100 nm (15%–25% of the surface area), while for the 2.2 μm period samples the ridges tend to be 100–200 nm in width (10%–20% of the surface area). Although the impact of ridge width is convoluted with ARC thickness and other factors, the general trend can be observed in Figure 1e–g that for $300 < \lambda < 500$ nm, the 2.2 μm samples with a smaller fraction of planar surface area exhibit superior absorption to the 700 nm pitch PIPs (see also Figure S1c in the Supporting Information).

The random pyramid samples offer some of the best results in the range $300 < \lambda < 500$ nm while tailing off in the infrared wavelengths for $\lambda > 800$ nm compared to the periodically textured samples (The 10 μm samples were outliers from the rest; the pyramid sizes of these samples were notably smaller than the other random samples (≈200–300 nm in height) and delivered overall lower absorptance.) The improved performance in the short wavelength range may be a function of the elimination of planar surface area for UPs, per the preceding discussion. It may also be influenced by the relatively small sizes of the random pyramids on these experimental samples, ranging in height from 300 to 700 nm. The somewhat lower long-wavelength performance is in part a result of decreased top-to-bottom peak thickness of the random samples. (For all sample types, the thickness referenced is the starting film thickness; owing to the fact that the random etching is done without any masking and the entire surface is etched in the process of forming pyramids—in contrast with the fabrication of the periodic textures—the maximum film height is reduced by 1–2 μm from the starting thickness.)

In spite of the differences in spectral absorption characteristics between the pyramidally textured samples, the total integrated absorption provided by the various surface light-trapping structures is very similar (**Figure 2**a). To convey full-spectrum absorption capability, we adapt the term photocurrent (J_{ph}) to represent the total absorption of the material stack (including parasitics) in units of current familiar to practitioners in the field of photovoltaics (mA cm^{-2}). J_{ph} is calculated as the inner product of the absorption and AM1.5G solar spectra, $A(\lambda)$ and $I_{AM1.5}(\lambda)$, respectively

$$J_{ph} = \left(\frac{q}{hc}\right)\int_0^{\lambda_g} \lambda * A(\lambda) * I_{AM1.5}(\lambda)\,d\lambda \quad (2)$$

where q is the elementary unit of charge, h is Planck's constant, and c is the speed of light in vacuum. Considering 5 μm silicon films as an illustrative example, the mean J_{ph} is 38.0 and 38.1 mA cm^{-2} for the 700 nm pitch PIPs and random pyramids, respectively, while for the 2.2 μm pitch PIPs it is slightly higher at 38.7 mA cm^{-2}. In each case, the large period inverted pyramids offer a slight advantage; however, the difference in absorption effectiveness between large and small period inverted pyramids and conventional random pyramids is small.

The similarity between these sample types is understandable since all approach the physical limits of total absorption in a thin film. From **Table 1** it can be seen that for all thicknesses

Table 1. Experimentally measured total absorption and estimated absorption in silicon compared with the Yablonovitch limit. "Total absorption" gives the best-measured value for empirically measured total absorption for samples with 700 nm pitch periodic inverted pyramids and the structure shown in Figure 1d. The right-most column represents the estimated absorption only in the silicon layer and is found by subtracting estimated parasitic absorption (using simulation data) from measured total absorption.

	J_{ph} [mA cm^{-2}]		
Silicon film thickness [μm]	Yablonovitch limit	Total absorption	Estimated silicon absorption
5	38.6	38.2	36.0
10	40.0	39.1	37.0
20	41.2	40.2	38.3

considered, the experimental samples fail to absorb at most 1 mA cm^{-2} of the photons that would be absorbed in the Yablonovitch limit (3 mA cm^{-2} if excluding absorption in the aluminum). A significant fraction of the difference between the experimental and Yablonovitch values for these samples originates in the spectral range $300 < \lambda < 500$ nm, where the Yablonovitch limit gives absorption values of better than 99.9% but reflection reduces absorption in the experimental samples. Although a compelling theoretical argument has been made that optimal periodic structures can always outperform random ones,[38] the finding that total absorption is similar in both random and periodic embodiments of a given geometry generally aligns with conclusions from other groups evaluating random and periodic textures in amorphous and microcrystalline silicon.[39–41] Efforts to produce high-efficiency thin-film silicon solar cells with conventional random pyramid textures have yielded very promising results, such as a 19.1% efficient solar cell on 43 µm silicon film[42] and a 16.8% device on a silicon film ≈21 µm thick,[43] offering further evidence that random pyramid textures compete favorably with nanophotonic designs.

The parameters driving the uniformly high absorption of these various pyramidal structures can be better understood through results from 3D finite element optical simulation, implemented using the wave optics module in COMSOL Multiphysics. By fixing the period of the inverted pyramid array at 700 nm and changing the pyramid angle, one finds that total integrated aborption in a thin silicon slab reaches a maximum in the vicinity of 55° (Figure 2b), nearly coincident with the angle provided by anisotropic alkaline etching of (100)-orientation silicon—54.7°. It is well known that a graded effective index of refraction tends to reduce reflection from a surface across all wavelengths, which is reflected in these results by rapidly rising total absorption with increasing pyramid angle. But spectral analysis indicates that the most pronounced effect of changing pyramid angle is on the short wavelength portion of the spectrum, $300 < \lambda < 500$ nm. In this range, the surface texture is large enough compared to the wavelength of light that the particle analogy of light from geometric optics can help visualize the way in which the angled sides of a given pyramid serve to reflect a normally incident electromagnetic wave back and forth while channeling it toward the bulk to increase the odds of absorption. As a result of these two effects—grading of the index change and short wavelength channeling—pyramidal geometries etched in silicon using alkaline solutions yield exceptionally high-light absorption. Nonetheless, additional improvements in absorption can be gained using techniques such as symmetry breaking and quasi-randomness.[13,20,21,36]

The size (pitch) of the surface texture is another variable expected to impact the total absorption effectiveness of the light-trapping structure. In Figure 2c, total integrated absorption is plotted for a 10 µm silicon film as a function of the pitch of inverted pyramid surface light-trapping structures, with the angle of the pyramid unit cell fixed at the potassium hydroxide (KOH) etch angle of 54.7°. Total absorption increases precipitously until reaching a local maximum around 700 nm. Interestingly, beyond a one-micrometer pitch, total absorption climbs back to a value slightly above that for 700 nm and remains steady. In spite of the greater volume of silicon that is removed for larger inverted pyramids, total absorption does not decline and even shows a somewhat positive trend for pitches larger than one micrometer.

The physical basis of the relationship between pitch size and total integrated absorption can be better understood and visualized through the absorption maps shown in **Figure 3**. Across

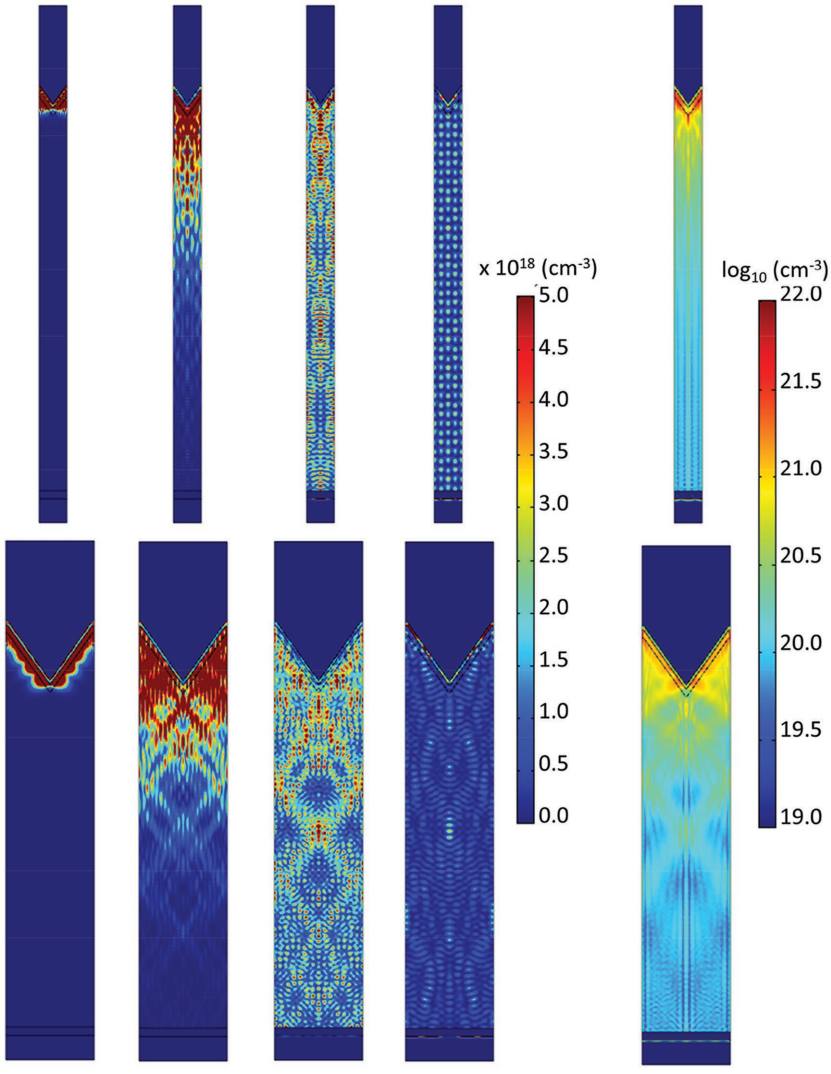

Figure 3. Spatial absorption profiles for 2D analogues of periodic inverted pyramids with pitches of a) 700 nm and b) 2.2 µm. Samples are modeled with a 100 nm PECVD nitride ARC, 250 nm silicon dioxide rear dielectric, an aluminum reflector, and a 50 nm ridge width separating inverted pyramids. 2D FEA simulation of the experimental structures was executed using the wave optics module of COMSOL Multiphysics.

Adv. Optical Mater. **2016**,
DOI: 10.1002/adom.201500667

the majority of the relevant solar spectrum, the morphology of the absorption pattern is similar for structures textured with both 700 nm and 2.2 μm PIPs, forming vivid interference patterns that result from the interaction between the multiplicity of diffraction channels (i.e., grating modes) permitted by the surface grating. It is only for long wavelengths—illustrated here at 1000 nm—that a distinct resonant beat pattern arises in the 700 nm pitch samples that is not apparent in the 2.2 μm pitch samples. The beat pattern is indicative of the limited number of diffraction channels permitted by the 700 nm pitch surface grating, the quantity of which and the associated diffraction angles (β_m) can be found according to[36,44,45]

$$\beta_m = \sin^{-1}\left(\frac{m\lambda}{n_2 d} + \frac{n_1 \sin\theta}{n_2}\right) \quad (3)$$

where m is the grating mode number; n_1 and n_2 are the refractive indices in air (with $n_1 = 1$) and silicon, respectively; d is the grating pitch; and θ is the angle of incidence (for normally incident radiation with $\theta = 0°$—as used in the simulation of Figure 3—the second term in parentheses drops out). At this wavelength, the diffraction channels available in the 700 nm pitch case are restricted to integers $m = 0, \pm1, \pm2$. Although the restricted number of modes can serve to limit outcoupling of radiation that has entered an absorber, it necessarily reduces the in coupling of incident radiation, meaning that less radiation is admitted into the absorber in the first place and the nanophotonic features are disadvantaged.[36] Nonetheless, given that photovoltaic energy conversion is a broad-spectrum application, even the small differences in absorption morphology at longer wavelengths average out to total absorption that is roughly comparable between surfaces textured with pyramids of different pitch greater than 700 nm.

The relatively constant, high absorption of PIP structures with pitches beyond ≈1200 nm can be understood by the fact that the interaction of such structures with the solar spectrum of relevance to silicon is largely on a geometric optics basis. For smaller pitch sizes, the total absorption potential tends to be more variable as wave optics descriptions are required for a greater and greater slice of the solar spectrum and grating and waveguide modes in the structures overlap with troughs and peaks in the solar spectrum. Another practical characteristic of nanophotonic PIPs is a proportionally larger planar area on the wafer surface compared to larger period inverted pyramids for a fixed ridge width (w), leading to higher reflection in the short wavelengths where $\lambda < 500$ nm. The sum total result of these effects is to lead to an optimal pitch for nanophotonic inverted pyramids of ≈700 nm, while micrometer-sized pyramids appear to be able to meet or exceed the nanophotonic results for a given ridge width.

The implications of the finding that pyramidal light-trapping features of diverse sizes and arrangements absorb comparably well, are significant to the study of light trapping for ultrathin crystalline silicon solar cells. First, it contradicts the assumption that wavelength-scale features are requisite for maximizing absorption in thin silicon slabs. Rather, high absorption values are obtainable using pyramidal features of a wide range of sizes. A principal benefit of this finding is that larger light-trapping features are typically more straightforward to fabricate, widening the range of lithographic and nonlithographic masking approaches with potential to produce effective periodic light-trapping structures inexpensively. Second, the finding that periodic and random pyramid structures absorb comparably well, suggests that lowest-cost fabrication approaches should drive surface texturing for crystalline silicon.

The experimental findings, indicating that total spectral absorption is similar between silicon films patterned with conventional random surface textures and PIPs, benefit other aspects of ultrathin silicon solar cell design. 2D and 3D integrated photonic and electronic transport simulations can now be built for device modeling with the confidence that periodic surface structures and boundary conditions can realistically capture the physics at play in randomly textured solar cells. At the same time, it is simple to conceptualize new manufacturing flows incorporating periodic light-trapping structures that could provide easier and less expensive fabrication for thin film devices compared to traditional random pyramid texturing techniques,[46] making the PIPs studied here a valuable tool in the development of efficient and inexpensive solar power.

Experimental Section

Sample Fabrication: Samples were fabricated using silicon-on-insulator (SOI) wafers (Vendor: Ultrasil; device layer: 5, 10, or 20 μm thick, p-type, ρ = 1–5 Ω cm; buried oxide layer: 250 nm thick; handle layer: 500 μm thick, p-type, ρ = 1–5 Ω–cm). 700 nm and 2.2 μm periodic surface textures were produced in a five-step process using semiconductor fabrication equipment:

1. Deposit a thin low-pressure chemical vapor deposition (LPCVD) silicon nitride on the top surface.
2. Pattern a 2D hole array in photoresist using projection lithography.
3. Etch the exposed nitride in a magnetically enhanced reactive ion etching tool using a CF_4/O_2 chemistry.
4. Using the nitride hard mask, etch self-limiting inverted pyramids into the silicon using a 20% KOH solution.
5. Remove the nitride hard mask in phosphoric acid at 165 °C.

The randomly textured surfaces were formed by first treating the surface in SunSource 68—a proprietary surfactant indicated to yield smaller pyramid heights (Air Products) —and then etched in a 4% KOH/2% IPA solution at 80 °C for 5–6 min.

All sample types were next coated with ProTEK B3 (Brewer Science) to prevent alkaline attack of the top surface of the wafer while windows were etched through the handle wafer using a 20% KOH solution, stopping on the buried oxide. After stripping the ProTEK film in acetone, the top surface of all samples was coated with a PECVD nitride (n = 1.9) antireflective film (thickness variable) and completed by sputtering a 300 nm aluminum film to serve as the back reflector.

Sample Characterization: Reflectance was measured using a Newport Oriel 74125 monochromator, a Newport Oriel 70672 integrating sphere, and a calibrated silicon photodiode (Newport Oriel 71675_71580) connected to a Newport 2036-R power meter. Light from the monochromator entered through the topmost port of the six-port sphere and passed through the sphere before encountering the sample die at the far port, which was angled at 8° using a custom-machined wedge. A custom-designed port with an 8° angle and the same Spectralon diffuse reflecting coating as the inside of the integrating sphere ensured that photons from high-order reflection modes were reflected into the sphere. The measurement was repeated using a diffuse reflective reference sample (Avian Technologies, FWS-99-02c) to convert the measured signal strength into absolute absorptance. Measurements were corroborated with a specular reflective sample (Thorlabs, PF20-03-G01).

Supporting Information

Supporting Information is available from the Wiley Online Library or from the author.

Acknowledgements

The information, data, and work presented herein were funded by the U.S. Department of Energy SunShot Initiative under Award No. DE-EE0005320 (for device simulation and fabrication) and the Nanoscale Science and Engineering Initiative of the National Science Foundation under NSF Award No. CMMI-0751621 through the Center for Scalable and Integrated Nanomanufacturing at U. C. Berkeley (for light-trapping structure manufacturing); see the Supporting Information for more information. Experimental devices were fabricated through the use of MIT's Microsystems Technology Laboratories (MTL). M.S.B. acknowledges the support of the Martin Family Society. The authors thank J. del Alamo and N. Fang for constructive advice on experimentation and device fundamentals, D. Ward, B. Bicchieri, P. Tierney, K. Broderick, E. Lim, K. Payer, D. Terry, V. Diadiuk, P. Zamora, and B. Alamariu from MTL for their assistance with sample fabrication, and H. Kane from Air Products for generously providing a sample of SunSource 68.

Received: November 12, 2015
Revised: January 15, 2016
Published online:

[1] S. Mehta, Greentech Media, <http://www.greentechmedia.com/articles/read/Global-2013-PV-Module-Production-Hits-39.8-GW-Yingli-Leads-in-Production-a> (accessed: February, 2015).
[2] D. M. Powell, M. T. Winkler, A. Goodrich, T. Buonassisi, *IEEE J. Photovolt.* **2013**, *3*, 662.
[3] SEMI, *International Technology Roadmap for Photovoltaic (ITRPV)*, 5th ed. <http://www.itrpv.net/.cm4all/mediadb/Reports%20downloads/ITRPV_2014_Roadmap_Revision1_140324.pdf> (accessed: November, 2014).
[4] D. Redfield, *Appl. Phys. Lett.* **1974**, *25*, 647.
[5] P. Campbell, M. A. Green, *J. Appl. Phys.* **1987**, *62*, 243.
[6] K. J. Yu, L. Gao, J. S. Park, Y. R. Lee, C. J. Corcoran, R. G. Nuzzo, D. Chanda, J. A. Rogers, *Adv. Energy Mater.* **2013**, *3*, 1401.
[7] K.-Q. Peng, X. Wang, L. Li, X.-L. Wu, S.-T. Lee, *J. Am. Chem. Soc.* **2010**, *132*, 6872.
[8] B. M. Kayes, H. A. Atwater, N. S. Lewis, *J. Appl. Phys.* **2005**, *97*, 114302.
[9] R. Khandelwal, U. Plachetka, B. Min, C. Moorman, H. A. Kurz, *Microelectron. Eng.* **2013**, *111*, 220.
[10] S. Jeong, M. D. McGehee, Y. Cui, *Nat. Commun.* **2013**, *4*, 2950.
[11] Y. M. Song, J. S. Yu, Y. T. Lee, *Opt. Lett.* **2010**, *35*, 276.
[12] K. X. Wang, Z. Yu, V. Liu, Y. Cui, S. Fan, *Nano Lett.* **2012**, *12*, 1616.
[13] S. E. Han, G. Chen, *Nano Lett.* **2010**, *10*, 4692.
[14] A. Mavrokefalos, S. E. Han, S. Yerci, M. S. Branham, G. Chen, *Nano Lett.* **2012**, *12*, 2792.
[15] G. Li, H. Li, J. Y. L. Ho, M. Wong, H. S. Kwok, *Nano Lett.* **2014**, *14*, 2563.
[16] E. Garnett, P. Yang, *Nano Lett.* **2010**, *10*, 1082.
[17] M. D. Kelzenberg, S. W. Boettcher, J. A. Petykiewicz, D. B. Turner-Evans, M. C. Putnam, E. L. Warren, J. M. Spurgeon, R. M. Briggs, N. S. Lewis, H. A. Atwater, *Nat. Mater.* **2010**, *9*, 239.
[18] P. Kowalczewski, M. Liscidini, L. C. Andreani, *Opt. Express* **2013**, *21*, A808.
[19] L. Hu, G. Chen, *Nano Lett.* **2007**, *7*, 3249.
[20] E. R. Martins, J. Li, Y. Liu, V. Depauw, Z. Chen, J. Zhou, T. F. Krauss, *Nat. Commun.* **2013**, *4*, 2665.
[21] J. Gjessing, A. S. Sudbø, E. S. Marstein, *J. Appl. Phys.* **2011**, *110*, 033104.
[22] L. C. Andreani, A. Bozzola, P. Kowalczewski, M. Liscidini, *Sol. Energy Mater. Sol. Cells* **2015**, *135*, 78.
[23] C. Schuster, A. Bozzola, L. C. Andreani, T. F. Krauss, *Opt. Express* **2014**, *22*, A542.
[24] L. Zeng, P. Bermel, Y. Yi, B. A. Alamariu, K. A. Broderick, J. Liu, C. Hong, X. Duan, J. Joannopoulos, L. C. Kimerling, *Appl. Phys. Lett.* **2008**, *93*, 221105.
[25] P. Bermel, C. Luo, L. Zeng, L. C. Kimerling, J. Joannopoulos, *Opt. Express* **2007**, *15*, 16896.
[26] M. A. Green, S. Pillai, *Nat. Photonics* **2012**, *6*, 130.
[27] K. R. Catchpole, A. Polman, *Opt. Express* **2008**, *16*, 21793.
[28] F. J. Beck, A. Polman, K. R. Catchpole, *J. Appl. Phys.* **2009**, *105*, 114310.
[29] R. Pala, J. White, E. Barnard, J. Liu, M. Brongersma, *Adv. Mater.* **2009**, *21*, 3504.
[30] H. A. Atwater, A. Polman, *Nat. Mater.* **2010**, *9*, 205.
[31] R. Dewan, D. Knipp, *J. Appl. Phys.* **2009**, *106*, 074901.
[32] E. Yablonovitch, *J. Opt. Soc. Am.* **1982**, *72*, 899.
[33] U. Rau, U. W. Paetzold, T. Kirchartz, *Phys. Rev. B* **2014**, *90*, 035211.
[34] M. A. Green, *Prog. Photovoltaics* **2002**, *10*, 235.
[35] Z. Yu, A. Raman, S. Fan, *Phys. Rev. Lett.* **2012**, *109*, 173901.
[36] Z. Yu, A. Raman, S. Fan, *Proc. Natl. Acad. Sci. USA* **2010**, *107*, 17491.
[37] D. M. Callahan, J. N. Munday, H. A. Atwater, *Nano Lett.* **2012**, *12*, 214.
[38] R. Dewan, S. Shrestha, V. Jovanov, J. Hüpkes, K. Bittkau, D. Knipp, *Sol. Energy Mater. Sol. Cells* **2015**, *143*, 183.
[39] C. Battaglia, C.-M. Hsu, K. Söderström, J. Escarré, F. J. Haug, M. Charrière, M. Boccard, M. Despeisse, D. T. L. Alexander, M. Cantoni, Y. Cui, C. Ballif, *ACS Nano* **2012**, *6*, 2790.
[40] U. W. Paetzold, M. Smeets, M. Meier, K. Bittkau, T. Merdzhanova, V. Smirnov, D. Michaelis, C. Waechter, R. Carius, U. Rau, *Appl. Phys. Lett.* **2014**, *104*, 131102.
[41] M. Peters, C. Battaglia, K. Forberich, B. Bläsi, N. Sahraei, A. G. Aberle, *Opt. Express* **2012**, *20*, 29488.
[42] J. H. Petermann, D. Zielke, J. Schmidt, F. Haase, E. G. Rojas, R. Brendel, *Prog. Photovolt: Res. Appl.* **2011**, *20*, 1.
[43] L. Wang, J. Han, A. Lochtefeld, A. Gerger, M. Carroll, D. Stryker, S. Bengston, M. Curtin, H. Li, Y. Yao, D. Lin, J. Ji, A. Lennon, R. Opila, A. Barnett, presented at Proc. 28th EU PVSEC, Paris, France, 3DV.1.12., September 30th–October 4th, **2013**, p. 2641.
[44] S. Mokkapati, K. R. Catchpole, *J. Appl. Phys.* **2012**, *112*, 101101.
[45] Z. Yu, A. Raman, S. Fan, *Opt. Express* **2010**, *18*, A366.
[46] J. Thorstensen, S. E. Foss, J. Gjessing, *Prog. Photovolt: Res. Appl.* **2014**, *22*, 993.